



1 Comparison of CSES ionospheric RO data with COSMIC measurements

2 Xiuying Wang¹, Wanli Cheng², Zihan Zhou¹, Song Xu¹, Dehe Yang¹, Jing Cui¹

3 1. Institute of Crustal Dynamics, China Earthquake Administration, Beijing, China

4 2. Xinyang Station, Henan Earthquake Administration, Henan, China

5 Corresponding author: Xiuying Wang

6 **Abstract:** CSES is a newly launched electric-magnetic satellite in China; its main scientific objective
7 is to monitor earthquake related disturbances in ionosphere. A GNSS occultation receiver (GOR) is
8 installed on the satellite to inverse electron density related parameters. In order to validate the
9 radio occultation (RO) data from GOR onboard CSES, a comparison between CSES RO and the co-
10 located COSMIC RO data is conducted to check the consistency and reliability of the CSES RO data
11 using measurements from February 12, 2018 to March 31, 2019. CSES RO peak values (N_mF_2), peak
12 heights (h_mF_2), and electron density profiles (EDPs) are compared with corresponding COSMIC
13 measurements in this study. The results show that: (1) N_mF_2 s between CSES and COSMIC are in
14 extremely good agreement with a correlation coefficient of 0.9891. The near zero bias between
15 the two sets is $0.01235 \times 10^5/\text{cm}^3$ with a RMSE of $0.3680 \times 10^5/\text{cm}^3$; and the relative bias is 2.14%
16 with a relative RMSE of 16.40%, which are in accordance with previous studies according to error
17 propagation rules. (2) h_mF_2 s between the two missions are also in very good agreement with a
18 correlation coefficient of 0.9379; the mean difference between the two sets is 0.73km with a RMSE
19 of 13.02 km, which is within the error limits of previous studies; (3) Co-located EDPs between the
20 two sets are generally in good agreements, but with a better agreement for data above 200km
21 than that below this altitude. Data at the peak height ranges show the best agreement, and then
22 data above the peak regions; data below the peak regions, especially at the altitude of about the
23 E layer, show relatively large fluctuations. It is concluded that CSES RO data are in good agreement
24 with COSMIC measurements, and the CSES RO data are applicable for most ionospheric-related
25 studies. However, particular attention should be paid to EDP data below peak regions in application.

26 **Key words:** CSES satellite; COSMIC mission; radio occultation; validation; ionosphere

27 1. Introduction

28 The first China Seismo-Electromagnetic Satellite (CSES), also called ZH-1 in China, has been
29 working for over 1 year since its launch on February 2, 2018. This satellite is the first spaced-based
30 platform in China for both the 3-D earthquake observation and geophysical field measurement; a
31 subsequent satellite of this series will be launched in 2022 and the engineering work is under way.
32 The primary scientific objectives of the CSES mission is to obtain world-wide data of space
33 environment of the electromagnetic field, ionospheric plasma and charged particles, to monitor
34 and study the ionospheric perturbations which may possibly associated with earthquake activity,
35 especially with those destructive ones, to support the research on geophysics, space sciences as
36 well as electric wave sciences and so on, and also to provide the data sharing service for
37 international cooperation and scientific community (Shen et al., 2018; Wang et al., 2019).

38 The CSES satellite is sun synchronous orbit with an inclination angle of 97.4° at the altitude
39 of 507 km. The local time of descending and ascending nodes are 1400 and 0200 respectively. It
40 takes about 94.6 minutes to complete a circular orbit, thus about 15 orbits per day. The revisiting



1 period of CSES is 5 days, which means the satellite will nearly repeat the orbits after 5 days. At
2 present, the observation range of the CSES satellite is mainly between -65° and $+65^\circ$ of
3 geographic latitudes.

4 There are eight Chinese payloads and one Italian payload onboard the CSES satellite,
5 belonging to 3 categories: (1) electromagnetic observations, including search-coil magnetometer
6 (SCM), electric field detector (EFD), and high precision magnetometer (HPM); (2) ionosphere
7 related observations, including GNSS occultation receiver (GOR), plasma analyzer package (PAP),
8 Langmuir probe (LAP), and tri-band beacon (TBB); (3) and high-energy particles observations,
9 including high energetic particle package (HEPP) and high energetic particle package detector
10 (HEPD), of which HEPD is provided by Italian Space Agency.

11 Of the eight payloads, four are related to ionospheric parameter observations. The GOR
12 payload onboard CSES is a GPS/BD2 receiver to inverse ionospheric electron densities according to
13 the radio wave refractivity when traversing the ionosphere. It is known that low Earth Orbit (LEO)
14 based GPS/GNSS radio occultation (RO) technique has been a powerful technique in ionosphere
15 monitoring; using this technique, the accurate electron density profiles (EDPs) in the ionosphere
16 can be derived with high vertical resolution on a global scale from bending information of the RO
17 signals (Kuo et al., 2004; Rocken et al., 2000; Schreiner et al., 1999). Therefore, many LEO satellites
18 were launched with RO payload after the pioneer RO experiment on GPS/MET mission (Hajj et al.,
19 1998; Schreiner et al., 1999), such as the CHAMP satellite (Jakowski et al., 2002; Wickert et al.,
20 2009), the GRACE satellites (Beyerle et al., 2005), the most famous COSMIC mission (Anthes et al.,
21 2008; Lei et al., 2007), and so on. The application of RO technique is also an important part of the
22 CSES satellite. Combining with the in situ electron density measurements onboard CSES, the CSES
23 RO retrieved electron densities can be used to study global scale ionospheric 3D images from the
24 bottom of the ionosphere to the altitude of the CSES satellite using the large amount of daily
25 occultation events. However, a complete and thorough validation of the RO measurements
26 obtained by the CSES satellite is a necessary work before the retrieved electron density profiles can
27 be used for ionospheric studies.

28 A primary comparison, between CSES and COSMIC using the global distribution of peak values
29 (N_mF_2) and peak height (h_mF_2) data, was carried out during the in-orbiting test period of the CSES
30 satellite, and the CSES N_mF_2 values were also compared with the measurements from 3 digisondes
31 in China (Cheng et al., 2018). Both the comparisons show that the CSES RO N_mF_2 data are generally
32 consistent with data from other measurements. However, as the comparisons are limited to the
33 peak values and the date coverage is only two months, a more complete validation is still required
34 to assess the consistency and reliability of the RO profiles obtained by the CSES satellite. A large
35 amount of RO profiles have been obtained so far by CSES, which provide enough data to implement
36 a more detailed validation work.

37 Validation of RO profiles is usually done by comparing the profiles with the measurements
38 from vertical ionosondes or incoherent scatter radars (ISRs). However, RO electron density profiles
39 above the F2 peak region cannot be validated by ionosonde observations due to the unreliable
40 extrapolating data at these altitudes. In addition, the uneven distribution of the ionosonde stations,
41 most located on inland and fewer in the oceans, restricts the global comparison work. Although
42 ISRs can be used to validate RO electron density profiles above F2 peak region, this comparison is
43 limited due to the relatively small number of ISR sites as well as their limited operating time.
44 Therefore, we will carry out the comparison work using the RO measurements from the COSMIC



1 dataset in this paper.

2 Validation of the COSMIC electron density measurements has been performed in numerous
3 studies using different measurements, such as the cross validation of the retrieved profiles from
4 nearby spacecraft in the same COSMIC mission (Schreiner et al., 2007), comparison with ground-
5 based ionosondes and ISRs (Cherniak and Zakharenkova, 2014; Chu et al., 2010; Chuo et al., 2011;
6 Habarulema et al., 2014; Kelley et al., 2009; Krankowski et al., 2011; Lei et al., 2007; McNamara
7 and Thompson, 2015), comparison with the in situ electron density measurements (Lai et al., 2013;
8 Pedatella et al., 2015; Yue et al., 2011), comparison with radio tomography data using space
9 climatology phenomenon (Thampi et al., 2011), comparison with ionospheric model IRI (Lei et al.,
10 2007; Wu et al., 2015; Yang et al., 2009), and so on. As COSMIC RO data have been extensively
11 validated and widely accepted for application, COSMIC RO data are used to validate the in situ
12 plasma density observations from the Swarm constellation (Lomidze et al., 2017). We therefore
13 also try to use the COSMIC RO dataset to validate CSES RO measurements because of its relative
14 large amount of data with globally spatial coverage. In addition, similar RO retrieved data from the
15 two sets also provides a unique opportunity to check the consistency and reliability of CSES profiles
16 except for N_mF_2 and h_mF_2 parameters.

17 In this study, the validation work is implemented by comparing CSES N_mF_2 , h_mF_2 , and data from
18 EDPs at some altitudes with corresponding COSMIC measurements, and the bias and RMSE
19 between the two sets are then calculated and estimated to evaluate the consistency and reliability
20 of CSES RO inversed data. Based on the results, an application suggestion is given on the CSES RO
21 data.

22 **2. Data and Method**

23 **2.1 CSES and COSMIC RO data**

24 **1. CSES RO data**

25 GOR payload onboard CSES can receive the dual frequencies from GPS (L1:
26 1575.42MHz±10MHz; L2: 1227.6MHz±10MHz) and DB2 (L1:1561.98MHz±2MHz; L2:
27 1207.14MHz±2MHz) to inverse atmospheric and ionospheric parameters with sampling rate of
28 100Hz and 20Hz respectively. Firstly, TECs from GPS to LEO are calculated from the carrier phase of
29 the dual frequencies; and then electron densities are retrieved from TECs using the Abel integration
30 transformation. The Abel integration method and assumptions used in RO inversion process have
31 been described in detail in many publications (Kuo et al., 2004; Lei et al., 2007; Schreiner et al.,
32 1999) and will therefore not repeat here.

33 The GOR payload onboard CSES started to work on February 12, 2018 and ionospheric radio
34 occultation (RO) measurements have been conducted since then. CSES RO inversed data are
35 divided into 5 levels: 0, 1, 2, 2A and 3. Level-0 is original data; Level-1 is physical quantity in time
36 order; Level-2 is physical quantity data with satellite orbital information and geomagnetic
37 coordinates, while Level-2A is similar with Level 2, but with higher precise orbital information; and
38 Level-3 is 2D structural data product from Level-2 and Level-2A, which can provide peak value, peak
39 height and EDP data.



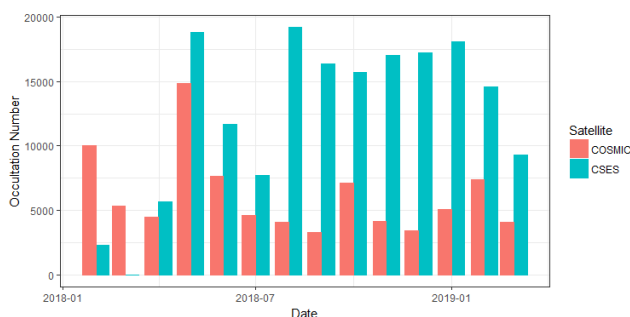
1 All the CSES RO data of the 5 levels are saved in HDF5 format, which is organized in a
2 hierarchical way. One file is saved for each occultation event, and about 500 to 600 occultation
3 event files can be obtained per day. Data users can refer to the data specification document for
4 detailed description of data file naming conventions and data level classification, which can be
5 obtained from the CSES data sharing center website www.leos.ac.cn.

6 More than 180,000 CSES occultation profiles have been obtained from 2018-02-12 to 2019-
7 03-31, of which occultation events co-located with that from the COSMIC mission will be used to
8 carry out the comparison and validation work in this paper.

9 2. COSMIC RO data

10 The COSMIC (Constellation Observing System for Meteorology, Ionosphere, and Climate, also
11 called FORMOSAT-3 in Taiwan) mission, a constellation of six identical low Earth orbit satellites
12 launched in April 2006, is a joint Taiwan-US mission to observe the near-real-time GPS RO data
13 (Anthes et al., 2008). COSMIC RO data come from the GPS Occultation Experiment (GOX) receivers
14 onboard the COSMIC satellites that monitor the two GPS L-band signals to establish the relative
15 geometries of satellite positions and differences in phase/Doppler shifts (Rocken et al., 2000). At
16 the University Corporation for Atmospheric Research (UCAR) COSMIC Data Analysis and Archive
17 Center (CDAAC), ionospheric profiles are retrieved by use of the Abel inversion technique from TEC
18 along LEO–GPS rays. Detailed description of CDAAC data processing and EDP retrieval method can
19 be found in some literatures (Kuo et al., 2004; Lei et al., 2007).

20 In the present study, the COSMIC level-2 electron density profiles provided as “ionPrf” files
21 from 2018-02-12 to 2019-03-31 are used, which can be downloaded from CDAAC website
22 <http://cdaa-www.cosmic.ucar.edu/>. COSMIC can provided over 2000-2500 RO profiles per day at
23 its initial stage, but for now only 200-300 events on average can be obtained each day. Fig.1 gives
24 the total occultation numbers of each month for both CSES and COSMIC missions from February
25 2018 to March 2019.



26

27 Fig. 1 Occultation number per month from February 2018 to March 2019 for both CSES and COSMIC

28 From Fig. 1 it can be seen that over 15,000 occultation events can be obtained by CSES each
29 month, or over 500 per day on average, after the initial in-orbit testing stage from February 2018
30 to July 2018. In contrast, occultation numbers from COSMIC are much less, there are only about
31 200 occultations on average each day. A total of over 86,000 occultation events have been obtained
32 from the COSMIC data center from February 2018 to March 2019.

33 Based on these two datasets from CSES and COSMIC, the co-located occultations within
34 defined spatial and temporal criteria from the two measurements are selected and used to carry
35 out the comparison work.

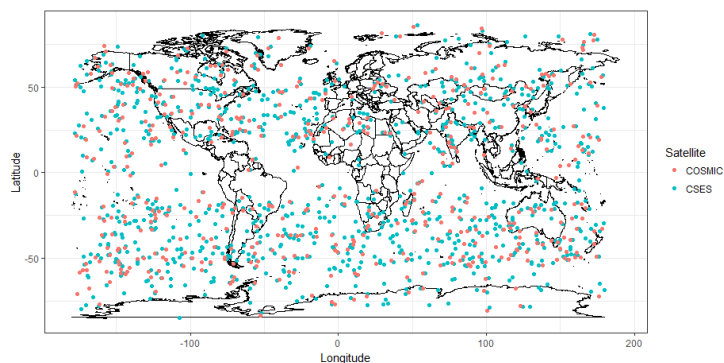


1 2.2 Data selection

2 In order to make the comparison between CSES and COSMIC RO data as accurate as possible,
3 spatial and temporal criteria must be defined to select matching occultation profiles for
4 subsequent comparison analysis.

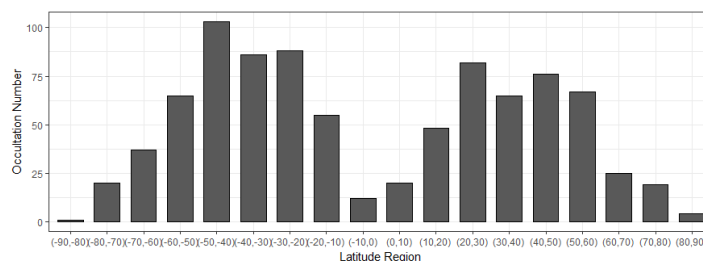
5 Before determining the selection criteria, it should be pointed out here that RO retrieved
6 electron density profiles cannot be interpreted as actual vertical profiles because both the LEO and
7 GPS are in motion during the occultation process. The geographic location of the tangent points of
8 a profile may vary in several hundred kilometers, which means the spatial range of a profile can
9 cover several degrees in horizontal latitude and longitude range, and several hundred kilometers
10 in vertical altitude range. However, the ionospheric spatial correlation can extent to a large area as
11 suggested by some researches (Shim et al., 2008; Yue et al., 2007). According to Shim et al. (2008),
12 the daytime meridional correlation lengths are approximately 9° and 5° at mid- and low-
13 latitudes, and the nighttime values are about 3° and 2° at mid- and low latitudes, respectively;
14 the zonal correlation lengths are 23° at mid-latitudes and 15° at low latitudes during the day,
15 and are 11° at mid-latitudes and 10° at low latitudes during the night. Therefore, the matching
16 profile pairs from the two missions must be within the correlation distances. Considering the
17 relatively small number of occultation events from the COSMIC measurements, we define the
18 search criteria for co-located occultation events as follows: (1) the time difference between the
19 matching occultation pairs is less than 30 min; (2) the distance differences between the locations
20 of the two occultation events are within $2^\circ \times 6^\circ$ range in latitudinal and longitudinal directions.
21 Here, the tangent point at F2 peak value of an occultation profile is defined as the location of the
22 occultation event. The reason to use the peak value tangent point as the occultation location is
23 because the peak value is normally located at the middle of a profile for the CSES EDPs, and by this
24 way the spatial differences of the corresponding points, especially the top and bottom points,
25 between the matching profile pairs can be limited to the correlation distance range as many as
26 possible.

27 Based on the above criteria, the RO profiles from CSES and COSMIC, covering the period from
28 February 2018 to March 2019, are searched to select the co-located profile pairs. The profiles with
29 $N_m F_2$ appearing below 150km or above 500 km are discarded, and profiles with only ascending or
30 descending part of a profile which cannot determine the peak values are also deleted from the
31 CSES dataset. A total of 891 matching profiles are found, and their distributions are given in Fig. 2.
32 Numbers of occultation in each 10 latitudinal region are also calculated and given in Fig.3.





1 Fig. 2 Distribution of the selected profile pairs
2 (Each dot indicates the location of the tangent point of the maximum values in a profile.)



3 Fig. 3 Number of co-located profile pairs along latitudinal regions
4

5 From Fig.2, it can be seen that the selected profile pairs are globally distributed, which makes
6 the data be representative of the whole dataset on spatial scale. In addition, the over a year
7 temporal segment, covering different periodic components of the ionospheric variations, makes
8 the data involved in the comparison be temporal representative also.

9 It is necessary to note that because the CSES satellite is sun-synchronous orbit as mentioned
10 earlier, the local time of the occultation events is concentrated around the ascending (0200) and
11 descending (1400) local time. Special attentions should be paid on the local time issue when CSES
12 and COSMIC RO data are combined together.

13 Another point to note is that most of the selected profile pairs are distributed in the mid-
14 latitude regions, as shown in Fig. 2 and Fig. 3, and the equatorial region as well as the high latitude
15 regions exhibit lower number of occultation events, which ensures that the selection criteria can
16 be satisfied for most of the selected matching profiles.

17 2.3 Comparison method

18 The CSES RO electron density data are compared with the co-located COSMIC RO data to assess
19 the consistency and reliability of the CSES RO data relative to that of the COSMIC, and then the
20 consistency and reliability of the CSES RO data relative to ground-based measurements are
21 estimated using the results obtained by previous researches on COSMIC RO data according to error
22 propagation rules.

23 The maximum electron density and its height, namely N_mF_2 and h_mF_2 from CSES RO data, are
24 compared and analyzed directly with the corresponding co-located COSMIC data, respectively.
25 Besides RO peak values, the profiles of the matching pairs are also compared in this study. To
26 compare the similarities of the profiles, average electron density data near some special altitudes
27 of a profile are calculated and compared. Because the orbit altitude of CSES is 507, only data below
28 this altitude are obtained from the CSES RO retrieved EDPs. Therefore, the special altitudes
29 involved in the comparison include 100, 150, 200, 250, 300, 350, 400, 450 and 500 km. The
30 consistency and reliability of the CSES RO profiles are thus evaluated by combining the comparison
31 results of these special altitudes.

32 Normally, the height resolution in the F region has the order of 20 km for the COSMIC RO (Kuo
33 et al., 2004), but CSES RO data has a higher resolution due to the higher sampling rate of the radio
34 signals. We therefore use the average data between the selected altitudes ± 10 km, which is just
35 within the vertical resolution of the COSMIC RO data.

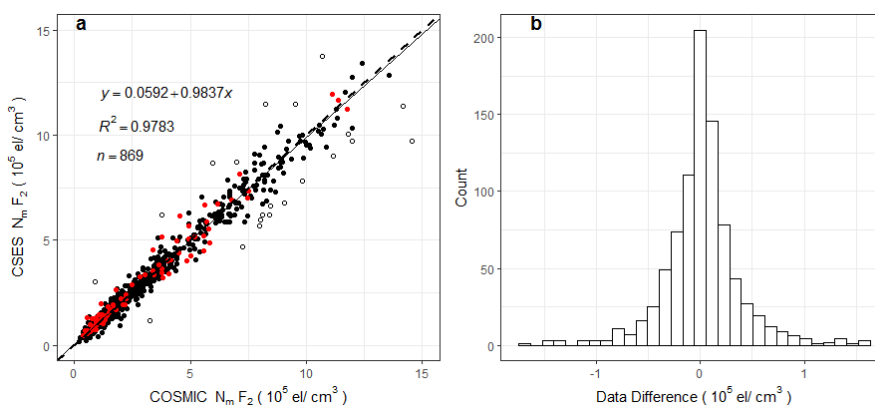


1 In this study, all the selected matching profiles are involved in the analysis rather than those
2 observed in geomagnetic quiet days. In this way, disturbed data caused by events such as
3 geomagnetic storms can also be used to compare their similarities/differences under these special
4 occasions.

5 3. Results and Discussions

6 3.1 Comparison of N_mF_2

7 The maximum electron density in the ionospheric F2 layer, N_mF_2 , is the most important
8 parameter in ionospheric related studies. To compare this parameter, the maximum electron
9 density data are extracted from all the matching RO files of CSES and COSMIC measurements.
10 Scatter plot of these matched N_mF_2 points is given in Fig. 4, also given is the histogram of the data
11 differences between the matched peak value points. As shown in Fig. 4b, data differences between
12 the two measurements are normally distributed; points with data differences exceeding 3 times
13 root mean square error (RMSE), shown as hollow circles in Fig. 4a, are considered outliers and can
14 be eliminated from the selected dataset according to 3σ rule. Red points in Fig. 4a are peak values
15 observed during geomagnetic storm conditions of $Dst < -30$ nT, all of which are within 3σ limits and
16 matched very good as shown in Fig. 4a. Fig. 4a also gives the linear fitting equation, the goodness-
17 of-fit coefficient R^2 (square of correlation coefficient), and number of data points.



18
19 Fig. 4 Scatter plot of matched N_mF_2 s and histogram of the data differences between the two sets
20 (The dash line in Fig. 4a is the equal value line with a slope of 1, and the solid line is the linear fitting line. Hollow
21 circles are points exceeding 3 times RMSE. Red solid points are data observed when $Dst < -30$ nT. y refers to CSES
22 N_mF_2 data, x COSMIC N_mF_2 data. R^2 is the goodness-of-fit coefficient; n is the total data number.)

23 The correlation coefficient between the matched N_mF_2 s with elimination of outliers is 0.9891,
24 and correlation coefficient without elimination of outliers is 0.9786, both of which can pass the
25 significance test of confidence level 0.01. The high correlation coefficient indicates the high
26 consistency between the two N_mF_2 sets. The linear fitting coefficient of 0.9837 given in Fig. 4a is
27 very close to 1; the data differences between the two sets are nearly normal distributed as shown



1 in Fig. 4b, and most of the data differences is around zero, all of which means that the CSES $N_m F_2$ s
 2 are nearly equal to COSMIC $N_m F_2$ s with a nearly zero bias. Both the correlation coefficient and the
 3 liner fitting coefficient indicate that the CSES $N_m F_2$ s are in extremely good agreement with the
 4 corresponding COSMIC data.

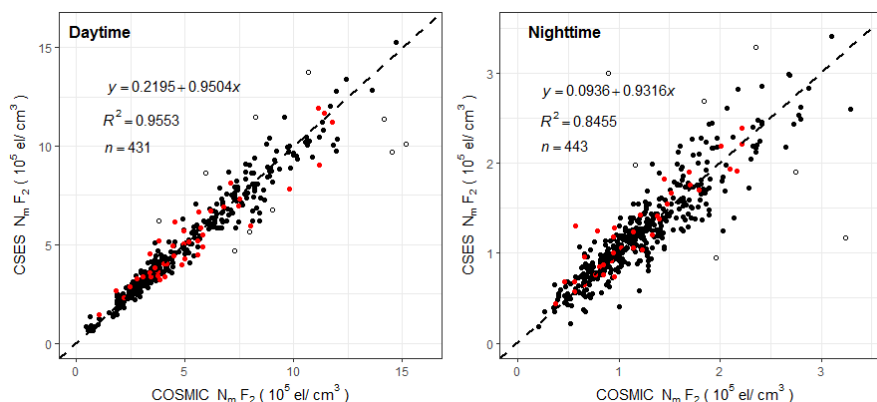
5 To quantify the error, we also calculate the RMSE and relative RMSE between the two sets. The
 6 mean of the data differences between CSES $N_m F_2$ and COSMIC $N_m F_2$ is $0.01235 \times 10^5 / \text{cm}^3$, and the
 7 RMSE between the two matched datasets is $0.3680 \times 10^5 / \text{cm}^3$, both of which are very small when
 8 comparing with the original data. Therefore, the nearly zero bias between the two measurements
 9 of $N_m F_2$ can be neglected, which is in accord with the normal distribution with most data
 10 differences clustering around zero as shown in Fig. 4b. The mean relative differences of $N_m F_2$
 11 calculated from equation (1) is 2.135%, and the corresponding relative RMSE is 16.40%. The mean
 12 relative data differences is also extremely small. The mean of data differences and the mean of
 13 relative data differences, as well as their RMSEs, again show that the CSES RO data are in very good
 14 agreement with the COSMIC data.

$$15 \quad E_r = \frac{1}{n} \sum_{i=1}^n \frac{z_i - y_i}{y_i} \times 100\% \quad (1)$$

16 Where z_i refers to the i th CSES $N_m F_2$ data of the matched data pairs, and y_i the corresponding
 17 COSMIC $N_m F_2$ data.

18 To compare the difference of correlation relationship for daytime and nighttime data, the data
 19 in Fig. 4 are divided into two groups. As introduced in section 2.2, the local time of CSES satellite is
 20 fixed at 0200 during night and 1400 during day, and the local time of RO data are around these two
 21 fixed local time, we therefore don't need to further consider differences caused by different local
 22 time.

23 The scatter plots for daytime and nighttime data are drawn using the same method introduced
 24 above and given in Fig. 5. The data obtained under geomagnetic storm conditions are also shown
 25 in red color, all of which are within the 3σ limits.



26
 27 Fig. 5 Scatter plot of $N_m F_2$ for daytime and nighttime data
 28 (the dash line in Fig. 5 is the equal value line with a slope of 1)

29 Correlation coefficient for daytime data with elimination of outliers is 0.9774, and 0.9637
 30 without elimination of outliers; for nighttime data with elimination of outliers, correlation



1 coefficient is 0.9195, and 0.8767 for all the data. The higher daytime correlation coefficient
2 indicates a better agreement for the daytime data than the nighttime data. This can be seen clearly
3 from Fig.5, the nighttime data are obviously fluctuated more violently.

4 The mean data differences for daytime data is $-0.01634 \times 10^5 / \text{cm}^3$ with a RMSE of $0.5572 \times$
5 $10^5 / \text{cm}^3$, and mean data differences for nighttime data is $0.01010 \times 10^5 / \text{cm}^3$ with a RMSE of
6 $0.2094 \times 10^5 / \text{cm}^3$. The opposite sign of the daytime and nighttime mean data differences indicates
7 that the CSES daytime data is slightly smaller than that of the COSMIC, while CSES nighttime data
8 is slightly greater than the corresponding COSMIC data, but both the means of data differences are
9 extremely small and can be consider zero bias when comparing when the original measurements.

10 Table 1 Absolute and relative error of $N_m F_2$ between CSES and COSMIC

	Correlation coefficient	Absolute Error		Relative Error	
		Mean ($/\text{cm}^3$)	RMSE ($/\text{cm}^3$)	Mean	RMSE
Total	0.9891	0.01235×10^5	0.3680×10^5	2.135%	16.40%
Daytime	0.9774	-0.01634×10^5	0.5572×10^5	1.344%	12.85%
Nighttime	0.9195	0.01010×10^5	0.2094×10^5	2.492%	18.70%

11 When comparing the different results given in Table 1, the absolute mean data differences for
12 daytime data is slightly greater than that of the overall result, and with an obvious larger RMSE;
13 while the mean data differences for nighttime data is slightly smaller than the overall result, and
14 also with a smaller RMSE. However, the two plots in Fig.5 indicate that the daytime data is obvious
15 better than the nighttime data. This is because the daytime data are much greater than nighttime
16 data, absolute error cannot correctly reflect the real situation when comparing data values with
17 different magnitudes. We therefore calculate the relative errors for both the daytime and nighttime
18 data. The mean relative data differences for daytime data is 1.344% with a relative RMSE of 12.85%,
19 and mean relative data difference for nighttime data 2.429% with a relative RMSE of 18.70%, which
20 indicate an obvious better agreement for the daytime measurements.

21 It is necessary to point out that most of the daytime data points with higher values are located
22 below the dash line as shown in Fig. 5, which means that the COSMIC $N_m F_2$ s are larger than that of
23 the CSES, so there is a negative bias between the two sets; while for nighttime data, most the data
24 points with higher values are above the dash line, indicating greater CSES $N_m F_2$ values, thus there
25 is a positive bias between them. This can also explain why there is a higher correlation coefficient
26 when combining daytime and nighttime data together.

27 There is another point to point out. As can be seen from Table 1, the absolute mean difference
28 for daytime data is negative, while the mean relative differences is positive. Further analysis shows
29 this different signs is caused by some points with much larger CSES $N_m F_2$ values.

30 Here, we compare our results with previous studies.

31 Lei et al. (2007) obtained a correlation coefficient of 0.85 when comparing COSMIC $N_m F_2$ with
32 observations from 31 globally distributed SPIDR (The Space Physics Interactive Data Resource,
33 <http://spidr.ngdc.noaa.gov/spidr>) ionosondes using data observed in July 2006. Chuo et al. (2013)
34 demonstrated that COSMIC derived $N_m F_2$ values are in good agreement with digisonde
35 observations of different seasons; they also reported an agreement about 0.96 using observations
36 from a lower latitude ionosonde in south hemisphere using a big dataset from May 2006 to April
37 2008. Chu et al. (2010) found a correlation coefficient of 0.98 when comparing $N_m F_2$ s between
38 COSMIC and 60 globally distributed ionosondes belonging to SWPC (Space Weather Prediction
39 Center), NOAA using data from November 2006 to February 2007. Krankowski et al. (2011)



1 obtained a very good correlation coefficient of 0.986 when validating COSMIC RO data in 2008
2 using measurements in European mid-latitude ionosondes. Our result of 0.9891 is quite similar to,
3 or even slightly better than those results, when considering the similar solar activity levels. A
4 relative high correlation coefficient between CSES N_mF_2 and ionosondes can be deduced since the
5 correlation transitive conditions are satisfied according to Langford et al. (2001). We therefore
6 obtained that CSES RO derived peak values are in very good agreement with COSMIC and ground-
7 based measurements.

8 For N_mF_2 relative errors, Krankowski et al. (2011) obtained a mean relative bias of 0.72% with a
9 standard deviation of 8.42%, and the slope of the linear fitting line is 0.994 using a manual
10 screening dataset in Europe, which is better than the results in this paper. Wu et al. (2009) got a -
11 3.2% relative bias with a standard deviation of 20.7% when comparing N_mF_2 s between COSMIC and
12 62 global ionosondes from SPIDR using data from July 2006 to Decemeber 2007. Yue et al. (2011,
13 2013) suggest that the ability to retrieve N_mF_2 using the Abel inversion technique has an
14 uncertainty about 10%. Based on the linear fitting equation between CSES and COSMIC and error
15 propagation rules, we can deduce that the relative errors between CSES peak values and ground-
16 based measurements are comparable to prior studies.

17 As to the absolute error, Kelley et al. (2009) obtained a RMSE of $1.0 \times 10^5 / \text{cm}^3$ when comparing
18 COSMIC data with ISR; Hajj et al. (2000) obtained a N_mF_2 RMS difference of about $1.5 \times 10^5 / \text{cm}^3$
19 when comparing the GPS/MET measurements with nearby ionosonde data, and Jakowski et al.
20 (2002) also obtained a similar RMS difference of about $0.9 \times 10^5 / \text{cm}^3$ when comparing the CHAMP
21 RO measurements to the in situ Langmuir probe data on the same satellite. Habarulema et al. (2014)
22 suggested that all RO data sets are close to the ionosonde data within similar error margin for both
23 mid-latitude and low-latitude regions when comparing COSMIC, GRACE and CHAMP RO data with
24 that of ionosondes. The absolute errors of our results are much smaller than these results, indicating
25 an extremely good agreements between CSES and COSMIC RO N_mF_2 and further confirming that
26 CSES RO are also within the general error limit as proposed by Habarulema et al. (2014).

27 Better result of daytime data in this study is in accord with the conclusion obtained by Wu et
28 al. (2009) and Yue et al. (2011). As we know, the nighttime data has a more complex spatial
29 distribution pattern compare to daytime data although daytime data are affected by solar radiation
30 during day time. Larger inversion error will be produced when facing uneven spatial distribution of
31 electron density due to the spherical symmetry assumption of the Abel inversion method. The
32 complex night time spatial distribution can also be proved by the smaller correlation distance
33 during nighttime than that of daytime as discussed in section 3.2 (Shim et al., 2008).

34 Besides data obtained under geomagnetic quiet days, data obtained under geomagnetic storm
35 conditions are also quite consistent with each other, this conclusion is also supported by the results
36 from Hu et al. (2014). They suggested that COSMIC measurements are acceptable under
37 geomagnetic disturbed conditions when comparing COSMIC RO data with observations from Sanya,
38 a lower latitude ionosonde in China.

39 As suggested by Schreiner et al. (2007) that co-located RO soundings allow the precision of the
40 technique to be estimated, but not the accuracy. That fact that the nearly zero bias for both
41 daytime and nighttime data and for the overall data, the normal distribution of the data differences,
42 as well as the extremely high correlation coefficient between CSES N_mF_2 and COSMIC N_mF_2 ,
43 demonstrates that the CSES N_mF_2 data are highly consistent and identical with COSMIC
44 measurements, even under geomagnetic storm conditions, indicating a similar precision of CSES

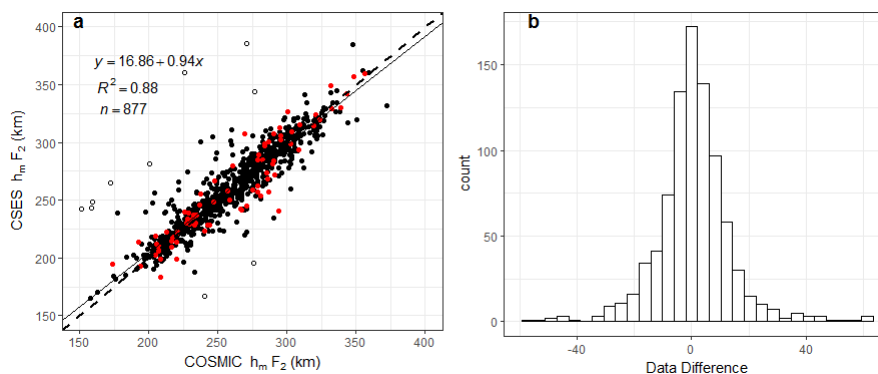


1 RO N_mF_2 data as that of COSMIC. Given the reliability (accuracy) of the COSMIC data proved by
2 many studies, we believe that the CSES N_mF_2 measurements are also quite reliable. Since the co-
3 located data points are globally distributed, the comparison results can be generalized to the
4 overall CSES N_mF_2 dataset obtained so far.

5 3.2 Comparison of h_mF_2

6 The height of the maximum peak values in F2 layer, h_mF_2 , is also a very important parameter
7 for ionospheric studies. We therefore also compare this parameter using the corresponding
8 COSMIC dataset.

9 Comparison of the h_mF_2 values between the two sets using the same method as that by N_mF_2 ,
10 the scatter plot of h_mF_2 and the histogram of the data differences are given in Fig. 6. Data points
11 exceeding 3 times of RMSE, shown as hollow circles in Fig. 6a, can be deleted from the selected
12 data sets when calculation is implemented. Again, all the peak height points obtained under
13 geomagnetic condition (red points) are within the 3σ limits as shown in Fig. 6a. It can be seen
14 clearly From Fig. 6a that most of the outliers (hollow circles) are obviously above the dash line,
15 which means that occasionally RO data from the CSES dataset will much overestimate h_mF_2 values.



16
17 Fig. 6 Scatter plot of h_mF_2 s for CSES and COSMIC and histogram of their differences

18 (The dash line is the equal values line with a slope of 1, and the solid line is the linear fitting line. y refers to the
19 CSES h_mF_2 , and x COSMIC h_mF_2 . Hollow circles are points exceeding 3 times standard deviation of data differences
20 between matched points. Red points are peak height obtained under geomagnetic condition of $Dst < -30$ nT.)

21 The correlation coefficient of h_mF_2 is 0.9379, though slightly lower than that of the N_mF_2 , but
22 can also pass the significance test of confidence level 0.01, which also indicates a very good
23 agreement between the two sets of h_mF_2 . The mean of the h_mF_2 data differences (CSES h_mF_2 minus
24 COSMIC h_mF_2) is 0.73 km, which indicates a slight greater h_mF_2 for the CSES peak height values; and
25 the RMSE is 13.02 km. h_mF_2 data difference between the two sets is so small, which can be regarded
26 as nearly zero bias.

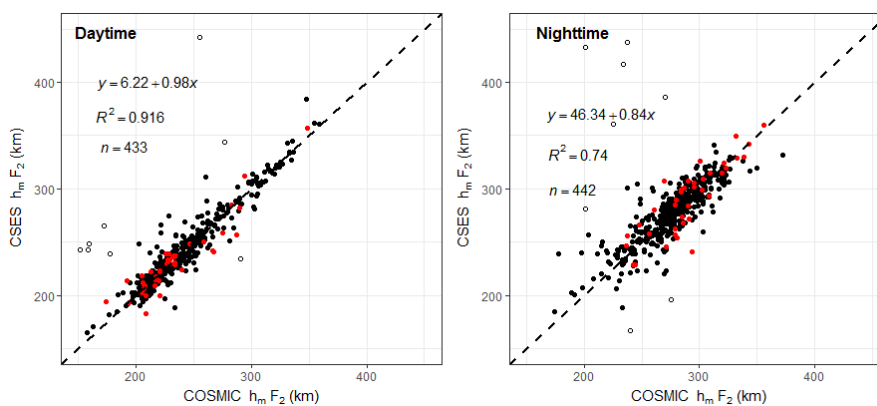
27 Compared with N_mF_2 , h_mF_2 data fluctuate more violently. It can be seen from Fig. 6a that some
28 data points are obviously deviated from the data cluster, or from the equal value dash line. Data
29 points above the dash line indicate that CSES h_mF_2 s are greater than the corresponding COSMIC
30 data, while data points below the dash line indicate a contrary situation that the COSMIC h_mF_2 s are
31 greater than that of CSES. Larger errors are produced by these obviously deviated situations. In



1 spite of the data fluctuation, the nearly zero bias between the two sets, namely the mean data
 2 differences, are so small that it can be neglected, which is in accord with the nearly normal
 3 distribution of data differences as shown in Fig. 6b. The high correlation coefficient and the
 4 normally distributed data differences again indicate that the overall $h_m F_2$ data of the two sets are
 5 in a good agreement.

6 We also compare the daytime and nighttime $h_m F_2$ s and the corresponding scatter plots are
 7 given in Fig. 7. Correlation coefficient for daytime data is 0.9571, and for nighttime 0.8592. Similar
 8 as $N_m F_2$, daytime $h_m F_2$ has a better correlation coefficient.

9 The mean data differences for daytime $h_m F_2$ s is 0.62km with a RMSE of 10.17km; while the
 10 mean data differences for nighttime $h_m F_2$ s is 0.84 with a RMSE of 14.81km. The positive means of
 11 data differences for both daytime and nighttime data indicate that the overall CSES $h_m F_2$ s are
 12 slightly greater than that of the COSMIC, but they are so small and can be neglected. The greater
 13 RMSE of the nighttime data indicates an obvious more fluctuating nighttime $h_m F_2$ s comparing to
 14 the daytime $h_m F_2$ s.



15
 16 Fig. 7 Scatter plot of $h_m F_2$ for daytime and nighttime data
 17 (the dash line in Fig. 5 is the equal values line with a slope of 1)

18 The bias and RMSE for overall, daytime and nighttime data are given in Table 2 for a comparison.

19 Table 2 Absolute error of $h_m F_2$ between CSES and COSMIC

	Correlation coefficient	Mean (km)	RMSE (km)
Total	0.9379	0.73	13.02
Daytime	0.9571	0.62	10.17
Nighttime	0.8592	0.84	14.81

20 From the results shown in Table 2 and Table 1, it can be seen that correlation of $N_m F_2$ is better
 21 than that of $h_m F_2$ between the two sets. This result is in accord with the conclusion that the RO
 22 measurements were better in $N_m F_2$ than in $h_m F_2$ (Chuo et al., 2011). Another point is that daytime
 23 $h_m F_2$ s are in better agreement than the nighttime data, which is similar as that of $N_m F_2$ data.

24 The overall comparison results of $h_m F_2$ are very good when comparing to prior validation
 25 studies using ionsondes observations. Chuo et al. (2013) reported an $h_m F_2$ agreement about 0.87
 26 using observations in low latitude south hemisphere from May 2006 to April 2008. Krankowski et
 27 al. (2011) got a correlation coefficient of 0.949 when comparing COSMIC $h_m F_2$ data observed in
 28 2008 with that from ionsondes in European mid-latitudes. Our result is consistent with their



1 results, which further proves that CSES h_mF_2 s are consistent and reliable with ionosondes
 2 observations.

3 Krankowski et al. (2011) also obtained a bias of 2.8km and a standard deviation of 11.5km for
 4 the COSMIC h_mF_2 data. Cherniak and Zakharenkova (2014) showed that COSMIC h_mF_2 s were in a
 5 good agreement with Kharkov ISR observations of different seasons in 2008-2009, and bias and
 6 standard deviations are less than 24 km and 29 km respectively. Habarulema et al. (2014) obtained
 7 an error limit about 30km when comparing COSMIC h_mF_2 s with mid-latitude ionosonde using data
 8 in 2008. Yue et al. (2011) suggested that the retrieval uncertainty in h_mF_2 is about 10km for COSMIC
 9 simulation analysis. The nearly zero bias and the small RMSE between h_mF_2 of CSES and COSMIC
 10 demonstrate that F region peak height parameter obtained by CSES and COSMIC are extremely
 11 similar with each other, we therefore deduce that error between CSES h_mF_2 and ionosondes h_mF_2 is
 12 comparable to prior results according to error propagation rules.

13 As a result, the significant correlation coefficient indicate the consistent variations between
 14 CSES h_mF_2 s and h_mF_2 s, and the nearly zero bias and the comparable error limits to prior studies
 15 further indicate that CSES RO inverted h_mF_2 s are reliable considering the reliability of COSMIC RO
 16 data validated by previous studies.

17 3.3 Comparison of EDPs

18 Besides the two most important parameters N_mF_2 and h_mF_2 , electron density profiles (EDPs) are
 19 also very important because EDPs can provide electron densities at different altitudes to depict
 20 ionospheric 3D images from the bottom of ionosphere to the altitude of LEO satellite.

21 As EDPs from CSES and COSMIC have different altitudes due to the different satellite altitudes
 22 of the two missions, only data under the altitude of the CSES satellite can be compared from the
 23 co-located profiles. We therefore compare the inversed data at some special altitudes as the
 24 numbers of data points are not identical for each matched profile pairs, and altitudes of each
 25 inversed data are not identical for the two co-located profile pairs either.

26 For each altitude specified in section 2.3, we calculate the correlation coefficients using all the
 27 matched data points at that altitude and the results are given in Table 3. Fig.8 gives the scatter
 28 plots of all these altitudes, and data obtained in geomagnetic date are shown in red points, also
 29 shown in the figure are the linear fitting equations, goodness-of-fit coefficients, and numbers of
 30 data points involved in the calculation. Outliers are eliminated from the data sets using the same
 31 criteria mentioned above.

32 Table 3 Correlation coefficients and RMSEs for the data at different altitudes of the profiles

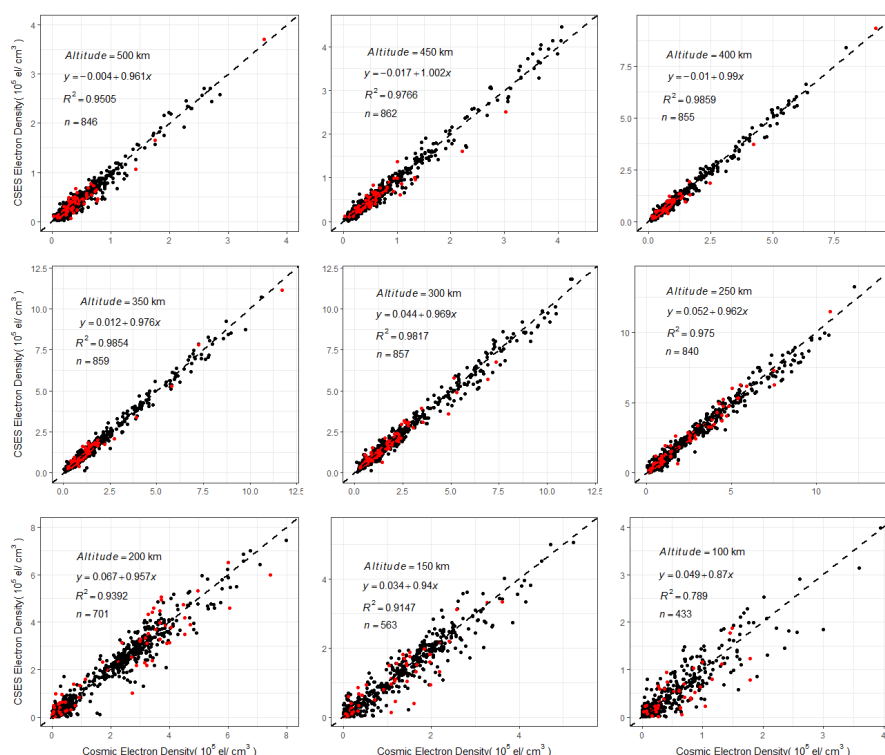
Altitude (km)	Correlation Coefficient	Absolute error		Relative error	
		Mean data difference	RMSE	Mean relative data differences	Relative RMSE
500	0.9749	-0.01982×10^5	0.8824×10^5	-1.716%	35.90%
450	0.9882	-0.01551×10^5	0.1070×10^5	-0.6894%	27.30%
400	0.9929	-0.01923×10^5	0.1314×10^5	-0.5888%	20.29%
350	0.9927	-0.02274×10^5	0.1946×10^5	0.7397%	23.45%
300	0.9908	-0.01881×10^5	0.2700×10^5	1.893%	25.16%
250	0.9874	-0.03198×10^5	0.3309×10^5	4.698%	61.29%
200	0.9691	-0.01090×10^5	0.3909×10^5	25.83%	133.8%



150	0.9564	-0.03161×10^5	0.2958×10^5	43.28%	324.7%
100	0.8883	-0.02330×10^5	0.2611×10^5	78.40%	519.0%

1 All the correlation coefficients in Table 3 can pass the significance test of confidence level 0.01,
2 which means that data points at different altitudes are highly correlated. When combining all the
3 results together, we can deduce that the co-located profiles from CSES and COSMIC sets are quite
4 similar to each other in spite of the global distribution of these profile pairs as shown in Fig. 2 in
5 Section 2.2. According to some studies, COSMIC profiles are in very good agreement with
6 observations from different ISRs (Lei et al., 2007; Kelley et al., 2009; Cherniak and Zakharenkova,
7 2014). Pedatella et al. (2015) compared COSMIC RO data at different altitudes with in situ
8 observations from CHAMP and C/NOSF and obtained the correlation coefficients are greater than
9 0.90, proving the consistency of the COSMIC profiles with in situ satellite observations. Based on
10 the high consistency between CSES and COSMIC profiles and prior COSMIC validation studies, we
11 can deduce that CSES profiles are generally agree with ISRs profiles according to similarity transitive
12 rules mentioned above (Langford et al., 2011).

13 Schreiner et al. (2007) showed that RMS is about $10^3/\text{cm}^3$ between 150 to 500km altitude,
14 whereas below 150km the RMS increases to a maximum of about $3 \times 10^3/\text{cm}^3$ at about 100km,
15 when comparing the RO profiles from different COSMIC satellites within 5km distance. Comparing
16 COSMIC profiles with ISR observations, Lei et al. (2007) suggested inversed errors are larger than
17 $10^5/\text{cm}^3$ at altitudes below $\sim 150\text{km}$ and Cherniak and Zakharenkova (2014) obtained an error range
18 of $12\text{-}16 \times 10^4/\text{cm}^3$. Pedatella et al. (2015) obtained an overall bias of $0.22 \times 10^5/\text{cm}^3$ with a
19 standard deviation of $0.65 \times 10^5/\text{cm}^3$, and relative bias and standard deviation are 14.9% and 10.4%
20 respectively, when validating COSMIC data at different altitudes using CHAMP in situ observations;
21 they also compared COSMIC data with C/NOFS in situ observations, and got a relative bias of 5.6%
22 with a standard deviation 12.4%. They attributed the better agreement with in situ observations
23 from C/NOFS to the higher altitude of this satellite. Both the absolute and relative errors, as well
24 as error variation with altitudes shown in Table 3, are in accord with those studies, suggesting that
25 the CSES EDPs are reliable and within general error limits due to the high similarity and consistency
26 between CSES and COSMIC EDPs.



1
 2
 3
 4
 5
 6
 7
 8
 9
 10
 11
 12
 13
 14
 15
 16
 17
 18
 19
 20
 21
 22

Fig. 8 Scatter plots of data from matched profiles at different altitudes
 (the dash line in Fig. 5 is the equal values line with a slope of 1)

From the correlation coefficients given in Table 3, it can be seen that correlation coefficients above 200 km are obviously greater than those below this altitude. The absolute mean differences at different altitudes are comparable to each other. However, relative differences at different altitudes are quite different; relative mean differences above 200km are extremely small, while relative mean differences below this altitude (include this altitude) increase dramatically. We obtained from Fig. 5 that the peak heights $h_m F_2$ of most profiles are located between 200km to 350km, the obviously high correlation coefficients in these regions indicate that RO inversed data at and above peak height are more consistent with each other, whereas discrepancies between the two data sets below the peak regions are much larger. This can be explained by the distribution characteristics of the different ionospheric layers, and by the spherical assumption used in Abel inversion method. As we know, electron density fluctuations in regions above the F2 peak become smaller under geomagnetic quiet conditions if comparing with that at lower altitudes due to the relative lower density according to electron density attenuation rules, it is therefore easier to satisfy the spherical symmetry assumption when using the Abel inversion method in this region. This spherical symmetry assumption is by far the most significant error source in the retrieval of the electron density profiles (Lei et al., 2007). In addition, a shorter propagating distance in the topside ionosphere for the radio signals from GPS to LEO will lead to a smaller error of straight line propagation assumption. As suggested by Liu et al. (2010) that COSMIC RO can obtain reasonable correct electron densities around and above F2 peak; however, assumption of spherical symmetry



1 introduces artificial plasma cave and plasma tunnel structures as well as electron density
2 enhancement at the geomagnetic equator at and below 250 km altitude, which will enlarge data
3 discrepancies as shown in Table 3. Syndergaard et al. (2006) also suggested larger errors at the
4 bottom of the retrieved profiles. The results shown in Table 3 in this study are in accord with those
5 studies, demonstrating that CSES EDPs have larger errors for data below 200km altitude, which is
6 similar as that of COSMIC.

7 An obvious characteristic shown in Table 3 is that all the means of data differences are negative
8 values though they are very small compare to the original measurements, which means the overall
9 CSES data at different altitudes are smaller than the corresponding COSMIC data. The all negative
10 mean data differences at different altitudes may indicate a possible systematic bias between the
11 two measurements. This systematic lower values at all altitudes is most likely caused by the first-
12 order estimation of the electron density at the altitude of the CSES satellite, rather than the spatial
13 differences of the co-located profile pairs, because spatial differences lead to random errors.
14 However, further confirmation of this error sources is required. It is also necessary to point out that
15 the signs of the mean relative data differences at altitudes ≥ 400 km are negative, similar as the
16 signs of the corresponding absolute errors; whereas the signs of the mean relative data differences
17 at altitudes below 400km are positive, just on the contrary to the signs of absolute mean data
18 differences. Further analysis shows that the opposite signs are caused by points where CSES data
19 are much larger than that of COSMIC, and thus lead to extremely larger relative errors, which
20 further indicates that data below the peak regions, especially below about 150km, fluctuate more
21 violently.

22 Besides spherical symmetry and straight line propagation assumptions, the larger discrepancies
23 at altitudes below peak regions can be explained by the different spatial locations of the matched
24 profiles. Although the peak values of co-located profile pairs are near each other according to
25 selection criteria, data points other than peak values on the matched profile pairs may exceed the
26 selection criteria and result in larger distances due to the different tangent point path of the
27 matched profile pairs. As a result, a larger distance will lead to larger discrepancy between the
28 corresponding data sets. In addition, the tangent point path of the matched profiles may have
29 different directions, which will lead to different inversion results because each inversed data
30 represents average electron densities along the radio ray path. In regions with large horizontal
31 gradients, the different ray path can cause obvious difference between the matched profiles. At
32 altitudes below 200km, especially below 150 km, sporadic E-layers can cause large horizontal
33 gradients, and then lead to large inversion error. Wu et al. (2009) suggested that the large relative
34 error below 150 km is due to the errors transferred from upper altitude (the F layer) and the very
35 small electron density at that altitude. They also suggested that the larger ray separations can
36 induce larger errors which can be transferred to low altitudes; phase measurement errors induce
37 small relative fluctuations on the electron density at the topside ionosphere, but can cause large
38 relative fluctuations at low altitude ionosphere, because small electron density at low altitude is
39 sensitive to the phase errors. It is therefore concluded that many sources can cause large errors for
40 measurements at altitudes below 150km, which as a result lead to the large discrepancies between
41 CSES and COSMIC RO data at the bottom of the ionosphere.

42 Based on the above analysis, we conclude that CSES profiles are generally consistent with
43 COSMIC data very well and are reliable for data applications. However, larger discrepancies are
44 found at lower altitudes between the two sets comparing to data differences at higher altitudes.



- 1 Therefore, special attention should be paid to data below 200km in applications due to the relative
- 2 large discrepancies between the two datasets.

3 4. Summary and Conclusions

4 Validation of the CSES RO data is carried out to estimate the consistency and reliability of the
5 CSES RO data using the globally distributed measurements from the COSMIC mission covering the
6 date range from February 12, 2018 to March 31, 2019 as COSMIC RO data have been widely
7 validated their consistency and reliability using data from different measurements in global scale.
8 Comparing CSES N_mF_2 , h_mF_2 , and EDP data at some special altitudes, with corresponding COSMIC
9 RO data, we obtain the following results.

- 10 (1) CSES N_mF_2 data are highly consistent with that from COSMIC with a correlation coefficient
11 of 0.9891. The mean data differences is $0.01235 \times 10^5/\text{cm}^3$ with a RMSE of $0.3680 \times$
12 $10^5/\text{cm}^3$; the relative mean differences is 2.1% with a relative RMSE of 16.4%. Correlation
13 between daytime N_mF_2 data is obviously better than that of nighttime N_mF_2 data.
- 14 (2) CSES h_mF_2 data are also very consistent with COSMIC data, with a correlation coefficients
15 of 0.9379. The bias between the two sets is 0.73 km with a RMSE of 13.02km. Again,
16 daytime h_mF_2 has a better correlation than nighttime data.
- 17 (3) Co-located profiles between CSES and COSMIC are generally consistent with each other
18 very well, with a better agreement for data at and above peak height regions (200km)
19 than those below this regions. For EDP data below 200 km altitude, special attention
20 should be paid due to the relative large discrepancies between the two sets.
- 21 (4) Based on the results of comparing COSMIC data with data from different measurements,
22 it is deduced that CSES RO data are within the error limits obtained by previous studies
23 according to error propagation rules.

24 GOX payload onboard CSES satellite can obtain over 500 occultation events each day, which
25 provide a large dataset for the study of 3D distribution of the ionospheric electron density when
26 combining with the in situ electron density measurements obtained by LAP onboard CSES. The
27 relatively thorough comparison work in this paper demonstrates that the CSES RO data are
28 consistent very well with the corresponding COSMIC data, proving that the CSES RO data are
29 reliable for applications on ionospheric-related problems. However, as many RO related studies
30 suggest that asymmetry of electron density distribution is the main source of the Abel inversion
31 transformation (Schreiner et al., 1999; Syndergaard et al., 2006; Lei et al., 2007), and this inversion
32 error varies with solar activity, season, geomagnetic latitude and local time (Wu et al., 2009). The
33 CSES RO data in this study cover all the latitudes and four seasons with fixed local time under lower
34 solar activity condition, and solar activity in this study is similar as most of the COSMIC validation
35 studies, the comparison results will therefore applicable to data with similar low solar activity
36 conditions. More subsequent validation work will be conducted and presented using data
37 accumulated under different solar activities.



1 Acknowledgement

2 COSMIC Radio Occultation data were downloaded from [ftp://cdaac-](ftp://cdaac-ftp.cosmic.ucar.edu/cosmic/level2/ionPrf/)
3 [ftp.cosmic.ucar.edu/cosmic/level2/ionPrf/](ftp://cdaac-ftp.cosmic.ucar.edu/cosmic/level2/ionPrf/). This research was supported by the National Key R&D
4 Program of China (Grant no. 2018YFC1503505), and by the Institute of Crustal Dynamics, China
5 Earthquake Administration (Grant no. ZDJ2018-18).

6 Reference

- 7 Anthes, R. A., Bernhardt, P. A., Chen, Y., Cucurull, L., Dymond, K. F., Ector, D., et al.: The COSMIC/FORMOSAT-3 Mission: Early
8 Results, *Bulletin of the American Meteorological Society*, 89(3), 313–334, doi:10.1175/bams-89-3-313, 2008.
- 9 Beyerle, G.: GPS radio occultation with GRACE: Atmospheric profiling utilizing the zero difference technique, *Geophysical*
10 *Research Letters*, 32, L13806, doi:10.1029/2005gl023109, 2005.
- 11 Cheng Y., Lin J., Shen X. H., Wan X., Li X. X., and Wang W. J.: Analysis of GNSS radio occultation data from satellite ZH-01, *Earth*
12 *and Planetary Physics*, 2(6), 499-504, <https://doi.org/10.26464/epp2018048>, 2018.
- 13 Cherniak, I. V., and Zakharenkova, I. E.: Validation of FORMOSAT-3/COSMIC radio occultation electron density profiles by
14 incoherent scatter radar data, *Advances in Space Research*, 53(9), 1304–1312, doi:10.1016/j.asr.2014.02.010, 2014.
- 15 Chu, Y.-H., Su, C.-L., and Ko, H.-T.: A global survey of COSMIC ionospheric peak electron density and its height: A comparison
16 with ground-based ionosonde measurements, *Advances in Space Research*, 46(4), 431–439, doi:10.1016/j.asr.2009.10.014,
17 2010.
- 18 Chuo, Y.-J., Lee, C.-C., Chen, W.-S., and Reinisch, B. W.: Comparison between bottomside ionospheric profile parameters
19 retrieved from FORMOSAT3 measurements and ground-based observations collected at Jicamarca, *Journal of Atmospheric and*
20 *Solar-Terrestrial Physics*, 73(13), 1665–1673, doi:10.1016/j.jastp.2011.02.021, 2011.
- 21 Chuo, Y. J., Lee, C. C., Chen, W. S., and Reinisch, B. W.: Comparison of the characteristics of ionospheric parameters obtained
22 from FORMOSAT-3 and digisonde over Ascension Island, *Annales Geophysicae*, 31(5), 787–794, doi:10.5194/angeo-31-787-2013,
23 2013.
- 24 Habarulema, J. B., Katamzi, Z. T., and Yizengaw, E.: A simultaneous study of ionospheric parameters derived from FORMOSAT-
25 3/COSMIC, GRACE, and CHAMP missions over middle, low, and equatorial latitudes: Comparison with ionosonde data, *Journal of*
26 *Geophysical Research: Space Physics*, 119(9), 7732–7744, doi:10.1002/2014ja020192, 2014.
- 27 Hajj, G. A., and Romans, L. J.: Ionospheric electron density profiles obtained with the Global Positioning System: Results from
28 the GPS/MET experiment, *Radio Science*, 33(1), 175–190, doi:10.1029/97rs03183, 1998.
- 29 Hu, L., Ning, B., Liu, L., Zhao, B., Chen, Y., and Li, G.: Comparison between ionospheric peak parameters retrieved from COSMIC
30 measurement and ionosonde observation over Sanya, *Advances in Space Research*, 54(6), 929–938,
31 doi:10.1016/j.asr.2014.05.012, 2014.
- 32 Jakowski, N., Wehrenpfennig, A., Heise, S., Reigber, C., Lühr, H., Grunwaldt, L., and Meehan, T. K.: GPS radio occultation
33 measurements of the ionosphere from CHAMP: Early results, *Geophysical Research Letters*, 29(10), 95-1–95-4,
34 doi:10.1029/2001gl014364, 2002.
- 35 Kelley, M. C., Wong, V. K., Aponte, N., Coker, C., Mannucci, A. J., and Komjathy, A.: Comparison of COSMIC occultation-based
36 electron density profiles and TIP observations with Arecibo incoherent scatter radar data, *Radio Science*, 44, RS4011,
37 doi:10.1029/2008rs004087, 2009.
- 38 Krankowski, A., Zakharenkova, I., Krypiak-Gregorczyk, A., Shagimuratov, I. I., and Wielgosz, P.: Ionospheric electron density



- 1 observed by FORMOSAT-3/COSMIC over the European region and validated by ionosonde data, *Journal of Geodesy*, 85(12), 949–
2 964, doi:10.1007/s00190-011-0481-z, 2011.
- 3 Kuo, Y.-H., Wee, T.-K., Sokolovskiy, S., Rocken, C., Schreiner, W., Hunt, D., and Anthes, R.: Inversion and Error Estimation of GPS
4 Radio Occultation Data, *Journal of the Meteorological Society of Japan*, 82(1B), 507–531, doi:10.2151/jmsj.2004.507, 2004.
- 5 Lai, P.-C., Burke, W. J., and Gentile, L. C.: Topside electron density profiles observed at low latitudes by COSMIC and compared
6 with in situ ion densities measured by C/NOFS, *Journal of Geophysical Research: Space Physics*, 118(5), 2670–2680,
7 doi:10.1002/jgra.50287, 2013.
- 8 Langford, E., Schwertman, N., and Owens, M.: Is the Property of Being Positively Correlated Transitive? *The American*
9 *Statistician*, 55(4), 322–325, doi:10.1198/000313001753272286, 2001.
- 10 Lei, J., Syndergaard, S., Burns, A. G., Solomon, S. C., Wang, W., Zeng, Z., et al.: Comparison of COSMIC ionospheric
11 measurements with ground-based observations and model predictions: Preliminary results, *Journal of Geophysical Research:*
12 *Space Physics*, 112, A07308, doi:10.1029/2006ja012240, 2007.
- 13 Liu, J. Y., Lin, C. Y., Lin, C. H., Tsai, H. F., Solomon, S. C., Sun, Y. Y., et al.: Artificial plasma cave in the low-latitude ionosphere
14 results from the radio occultation inversion of the FORMOSAT-3/COSMIC, *Journal of Geophysical Research: Space Physics*, 115,
15 A07319, doi:10.1029/2009ja015079, 2010.
- 16 Lomidze, L., Knudsen, D. J., Burchill, J., Kouznetsov, A., and Buchert, S. C.: Calibration and Validation of Swarm Plasma Densities
17 and Electron Temperatures Using Ground-Based Radars and Satellite Radio Occultation Measurements. *Radio Science*, 53(1), 15–
18 36, doi:10.1002/2017rs006415, 2018.
- 19 McNamara, L. F., and Thompson, D. C.: Validation of COSMIC values of foF2 and M(3000)F2 using ground-based ionosondes.
20 *Advances in Space Research*, 55(1), 163–169, doi:10.1016/j.asr.2014.07.015, 2015.
- 21 Pedatella, N. M., Yue, X., and Schreiner, W. S.: Comparison between GPS radio occultation electron densities and in situ satellite
22 observations, *Radio Science*, 50(6), 518–525, doi:10.1002/2015rs005677, 2015.
- 23 Rocken, C., Kuo, Y.-H., Schreiner, W., Hunt, D., Sokolovskiy, S., and McCormick, C.: COSMIC system description, *Terr. Atmos.*
24 *Ocean Sci.*, 11(1), 21–52, DOI: 10.3319/TAO.2000.11.1.21(COSMIC), 2000.
- 25 Schreiner, W., Rocken, C., Sokolovskiy, S., Syndergaard, S., and Hunt, D.: Estimates of the precision of GPS radio occultations
26 from the COSMIC/FORMOSAT-3 mission, *Geophysical Research Letters*, 34, L04808, doi:10.1029/2006gl027557, 2007.
- 27 Schreiner, W. S., Sokolovskiy, S. V., Rocken, C., and Hunt, D. C.: Analysis and validation of GPS/MET radio occultation data in
28 the ionosphere, *Radio Science*, 34(4), 949–966, doi:10.1029/1999rs900034, 1999.
- 29 Shen, X., Zhang, X., Yuan, S., Wang, L., Cao, J., Huang, J., et al.: The state-of-the-art of the China Seismo-Electromagnetic
30 Satellite mission, *Science China Technological Sciences*, 61(5), 634–642, doi:10.1007/s11431-018-9242-0, 2018.
- 31 Shim, J. S., Scherliess, L., Schunk, R. W., and Thompson, D. C.: Spatial correlations of day-to-day ionospheric total electron
32 content variability obtained from ground-based GPS, *Journal of Geophysical Research: Space Physics*, 113, A09309,
33 doi:10.1029/2007ja012635, 2008.
- 34 Syndergaard, S., W. S. Schreiner, C. Rocken, D. C. Hunt, and K. F. Dymond: Preparing for COSMIC: Inversion and analysis of
35 ionospheric data products, in *Atmosphere and Climate: Studies by Occultation Methods*, edited by U. Foelsche, G. Kirchengast,
36 and A. K. Steiner, pp. 137–146, Springer, New York, 2006.
- 37 Thampi, S. V., Yamamoto, M., Lin, C., and Liu, H.: Comparison of FORMOSAT-3/COSMIC radio occultation measurements with
38 radio tomography, *Radio Science*, 46, RS3001, doi:10.1029/2010rs004431, 2011.
- 39 Wang, X., Cheng, W., Yang, D., and Liu, D. Preliminary validation of in situ electron density measurements onboard CSES using
40 observations from Swarm Satellites, *Advances in Space Research*, doi:10.1016/j.asr.2019.05.025, 2019.
- 41 Wickert, J., Michalak, G., Schmidt, T., Beyerle, G., Cheng, C.-Z., Healy, S. B.: GPS Radio Occultation: Results from CHAMP, GRACE
42 and FORMOSAT-3/COSMIC, *Terrestrial, Atmospheric and Oceanic Sciences*, 20(1), 35–50, doi:10.3319/tao.2007.12.26.01(f3c),
43 2009.
- 44 Wu, X., Hu, X., Gong, X., Zhang, X., and Wang, X.: Analysis of inversion errors of ionospheric radio occultation, *GPS Solutions*,



- 1 13(3), 231–239, doi:10.1007/s10291-008-0116-x, 2009.
- 2 Wu, K.-H., Su, C.-L., and Chu, Y.-H.: Improvement of GPS radio occultation retrieval error of E region electron density: COSMIC
3 measurement and IRI model simulation, *Journal of Geophysical Research: Space Physics*, 120(3), 2299–2315,
4 doi:10.1002/2014ja020622, 2015.
- 5 Yang, K.-F., Chu, Y.-H., Su, C.-L., Ko, H.-T., and Wang, C.-Y.: An Examination of FORMOSAT-3/COSMIC Ionospheric Electron
6 Density Profile: Data Quality Criteria and Comparisons with the IRI Model, *Terrestrial, Atmospheric and Oceanic Sciences*, 20(1),
7 193–206, doi:10.3319/tao.2007.10.05.01(f3c), 2009.
- 8 Yue, X., Schreiner, W. S., Kuo, Y.-H., Wu, Q., Deng, Y., and Wang, W.: GNSS radio occultation (RO) derived electron density
9 quality in high latitude and polar region: NCAR-TIEGCM simulation and real data evaluation, *Journal of Atmospheric and Solar-*
10 *Terrestrial Physics*, 98, 39–49, doi:10.1016/j.jastp.2013.03.009, 2013.
- 11 Yue, X., Schreiner, W. S., Rocken, C., and Kuo, Y.-H.: Evaluation of the orbit altitude electron density estimation and its effect
12 on the Abel inversion from radio occultation measurements, *Radio Science*, 46, RS1013, doi:10.1029/2010rs004514, 2011.
- 13 Yue, X., Wan, W., Liu, L., and Mao, T.: Statistical analysis on spatial correlation of ionospheric day-to-day variability by using
14 GPS and Incoherent Scatter Radar observations, *Annales Geophysicae*, 25(8), 1815–1825, doi:10.5194/angeo-25-1815-2007,
15 2007.